The effects of turmeric on the grain structure and properties of copper electrodeposited composites

Merrill, R. J., Wu, L., Graves, J., Beddow, J., Fuentes, E. & Cobley, A.

Author post-print (accepted) deposited by Coventry University's Repository

Original citation & hyperlink:
Merrill, RJ, Wu, L, Graves, J, Beddow, J, Fuentes, E & Cobley, A 2020, 'The effects of turmeric on the grain structure and properties of copper electrodeposited composites', Transactions of the Institute of Materials Finishing, vol. 98, no. 6, pp. 328-335.
https://dx.doi.org/10.1080/00202967.2020.1827588

DOI 10.1080/00202967.2020.1827588
ISSN 0020-2967

Publisher: Taylor and Francis

This is an Accepted Manuscript of an article published by Taylor & Francis in Transactions of the Institute of Materials Finishing on 11/11/2020, available online: http://www.tandfonline.com/10.1080/00202967.2020.1827588

Copyright © and Moral Rights are retained by the author(s) and/ or other copyright owners. A copy can be downloaded for personal non-commercial research or study, without prior permission or charge. This item cannot be reproduced or quoted extensively from without first obtaining permission in writing from the copyright holder(s). The content must not be changed in any way or sold commercially in any format or medium without the formal permission of the copyright holders.

This document is the author's post-print version, incorporating any revisions agreed during the peer-review process. Some differences between the published version and this version may remain and you are advised to consult the published version if you wish to cite from it.

Manuscript cover

The effects of turmeric on the grain structure and properties of copper electrodeposited composites

Richard. Merrill[a,*], Liang. Wu[a], John. E. Graves[a], Jamie. Beddow[a], Elena.Fuentes[b], Andrew. Cobley[a]

[a]The Functional Materials Research Group, Institute for Future Transport and Cities, Coventry university, Priory Street, Coventry, CV1 5FB, United Kingdom

[b]TEKNIKER, Parke Teknologikoa, C/IñakiGoenaga 5, 20600 Eibar, Gipuzkoa (Spain)

Abstract: This research aimed to electrocodeposit turmeric particles into copper matrices, and assess the influence of turmeric on the microstructure and properties of those deposits. The incorporation of turmeric had a significant effect on both the grain structure and properties of the copper deposits, with turmeric particles of a Z-average size of 289 ± 30 nm and 278 ± 15 nm having a greater influence on grain refinement than particles of 134 ± 37 nm, even at much lower deposit particle contents. The incorporated turmeric increased both the hardness and water contact angle of the deposits, however, a reduced in resistance to salt spray corrosion was also observed.

Keywords : Electrodeposition, copper, turmeric, sustainable, composite, microstructure.

1. Introduction

Material selection is a vital part of any engineering project. The correct selection (to meet the desired performance characteristics while minimizing cost) can be the difference between the success and failure of the project [1,2]. For certain applications, the desired performance characteristics may only be required at the surface of the material, in which case a surface coating can be utilised. Surface coatings can modify the surface properties of a material without changing the bulk properties; as such they offer a cost-effective solution to many engineering problems. They are essential for many industries including automotive, aerospace, construction, energy, healthcare, mining, transport, textiles, and even food and drink [3]. A report by the Surface Engineering and Advanced Coatings (SEAC) special interest group stated that the surface engineering and advanced coatings industry was worth £11 billion per annum to the UK economy, and effected products worth £140 billion [3].

One metal commonly utilised as a surface coating, due to its unique properties is copper. Copper has been employed by humans for thousands of years. It is a soft ductile metal, is highly electrical and thermally conductive, has strong antibacterial properties and is non-magnetic. Copper coatings are often used for heat exchangers, printed circuit boards, antibacterial surfaces, and decorative finishes [4-6].

For certain applications pure metal coatings may be insufficient for the required task, in these cases a composite coating may be used. The incorporation of inert particles into a metal matrix can enhance the properties of the material. However composite materials (as both coatings and bulk materials) are not without drawbacks. The incorporated particles can be of high cost and/or require complex manufacturing methods to produce. Due to the inherent heterogeneous nature of the matrix with filler material, composite materials can be extremely difficult to recycle (both for matrix and filler particles) compared to their single material counterparts [7]. These problems can make composite coatings expensive and unsustainable. One possible solution is to utilise a more sustainable source of filler particle. Recent research

has shown that the codeposition of the common kitchen spice turmeric into a nickel matrix significantly enhanced the hardness, water contact angle (WCA) and corrosion resistance of the material [8].

This present research aimed to produce a more sustainable copper composite coating by using the electro-co-deposition of turmeric, and to assess how turmeric affected the grain structure and properties of the deposit.

2. Materials and method

2.1. Particle size

The particle size of the turmeric in solution was measured with a Zetasizer nano S (Malvern instruments Ltd, Malvern Ltd) using a dynamic light scattering (DLS) technique. An electrolyte mimic was used to allow identification of turmeric particles in solution, which consisted of a 3.7 mol/L of H_2SO_4 supplied by Sigma Aldrich UK Ltd. Between 1.0 g/L and 10.0 g/L of turmeric supplied by Healthy Supplies UK Ltd with 10.0 ml/L of the surfactant Tween 20 supplied by Sigma Aldrich UK Ltd was added to the electrolyte mimic. The solutions were dispersed by ultrasound using a 20 kHz Sonic Systems sonic processor P100/3-20 horn model GA99893 for 20 min. Ultrasound power was varied from 11 W/L to 33 W/L to achieve specific particle sizes at different concentrations, allowing the relationship between turmeric particle size and concentration to be examined. Three drops of the solutions were added to 2.0 ml of Deionised water (DI) in a cuvette and the Z-average size measured at a refraction index of 1.4151. Each measurement consisted of 12 individual measurements of a minimum of 10 s duration. A cumulate analysis correlation function was used to obtain the intensity weighted mean of the hydrodynamic particle size (Z-average size). Three measurements for each sample were obtained and their mean values calculated.

2.2. Materials and method

To achieve a good quality homogeneous copper deposit of 30 μm at a cathode efficiency of 100%, the following conditions were selected. Direct current (DC) was utilised at a current density of 0.04 A /cm^2 at ambient room temperature for 36.5 min. A 35 mm magnetic stirring bar was used throughout deposition at a speed of 200 rpm. Previous research had demonstrated that high metal ion concentrations in the electrolyte can cause salting out of the turmeric particles, therefore a low metal ion concentration acid copper electrolyte was used [8]. The copper electrolyte was an aqueous solution of 75.0 ± 1.0 g/L of $CuSO_4.6H_2O$ supplied by Fisher Scientific UK Ltd, 1.6 x 10^{-2}mol/Lof HCl supplied Sigma Aldrich UK Ltd, and 3.7 mol/L of H_2SO_4. Tween 20 is a non-ionic surfactant commonly utilised for biochemical applications, previous research had demonstrated its effectiveness at dispersing turmeric particles in an electrolyte [8]. Between 1.0 g/L and 10.0 g/L of turmeric with 10.0 ml/L of Tween 20 was added to the copper electrolyte. The experimental setup is illustrated in Fig 1. Before deposition the turmeric particles were dispersed using ultrasound from a 20 kHz Sonic Systems sonic processor P100/3-20 horn model GA99893 for 20 min at a power of 11 and 33 W/L. A brass sheet 0.9 mm thick with a plating area of 25 mm^2 was used as the cathode, with a pure copper anode. An aqueous solution of 10 % Decon supplied by Sigma Aldrich UK Ltd, at ambient room temperature was used to remove any surface contaminants from the anode and cathode. To remove the oxidation layer the cathode and anode were submerged in a 3.9 M solution of H_2SO_4 at ambient room temperature for 60 s. DI water was then used to rinse off cathode and anode before electrodeposition. [fig 1. near here]

2.3. Microstructure

The primary constituent of turmeric is carbohydrates ($(CH_2O)_n$) at 67 %, other organic components are present (such as essential oils, proteins, fats, and curcuminoids) [9,10]. The carbon composition of the electrodeposits was examined with a GD Profiler 2 (HORIBA Jobin Yvon) RF Glow Discharge Optical Emission Spectrometer (GDOES) to assess their turmeric content. This was then compared to a control sample, electrodeposited from the

copper electrolyte containing only Tween 20. The effect of turmeric on the grain structure of the electrodeposits was then examined. A Zeiss sigma 500 VP scanning electron microscope (SEM) was utilised to obtain high resolution images of the surface of the electrodeposits. A FEI versa 3D FIB-SEM focused ion beam scanning electron microscope was utilised to obtain high resolution images of the cross section of the electrodeposit. The Ion beam images were then examined using ImageJ software to assess particle content and calculate the grain size using the line intercept method [8, 11].

$$Gs = \frac{l}{n} \tag{1}$$

Where *Gs* is the grain size in nm, *l* is the line length in nm, and n is the number of grains that intercept the line.

2.4. Properties

To assess the influence turmeric had on the deposits, the hardness, wetting behaviour, and corrosion resistance were examined. A Kruss DSA 100 drop shape analysis system was utilised to assess the wetting behaviour of the electrodeposits by their water contact angle (WCA). A DI water droplet of 2.0 µl was applied to 6 random positions on the surface of the electrodeposits. A Mitutoyo MVK-H1 microhardness testing machine with a Vicker's indenter was used to assess the electrodeposits hardness at 7 random positions. An Ascott cc ip 1000 salt spray chamber was utilised to assess the salt spray corrosion rate of the electrodeposits. The method used was adapted from ASTM B 117 – 03, Standard Practice for Operating Salt Spray (Fog) Apparatus. A 5.0 % wt NaCl solution was used, each electrodeposit was pre-weighed and placed in the salt spray chamber for 240 hours, the electrodeposits were washed with DI water, dried and re-weighed. The mass lost was used to calculate the corrosion rate (C_R) using equation 2.

$$C_R = \frac{k\,W}{A\,t\,d} \tag{2}$$

Where k is a constant that defines the units of the corrosion rate ($3.45e^6$ m/year), W is the mass lost in g, A is the area exposed to the salt spray in cm^2 ($2.5\ cm^2$), t is time in hours, and d is the density of copper.

3. Results and discussion

3.1 Particle size

[fig 2. near here]

The turmeric particle size was assessed by DLS to identify how turmeric concentration and sonication power affected particle size. The turmeric particle size in the copper electrolyte mimic measured by DLS is presented in Fig 2. The scattered-light intensity-weighted mean of the hydrodynamic particle diameter (Z-average size) progressively increased with increasing turmeric concentration up to 10.0 g/L (up to 900 ± 184 nm). Increasing applied ultrasound power to the 10.0 g/L solution from 11 W/l to 33 W/L, achieved a particle size within error of that seen for the 5.0 g/L solution (278 ± 15 nm and 289 ± 30 nm respectively). The application of low-frequency ultrasound to a liquid can cause acoustic cavitation, cavitation fields, micro-jetting (acoustic streaming, and high-speed particle collisions), breaking the weak van der Waals forces, dispersing and deagglomerating the particles [12-14]. Low-frequency ultrasonic waves propagate through liquid media by a series of compression and rarefaction cycles. During the rarefaction cycle (if power is sufficient) expansion forces caused by the ultrasound will exceed that of the intermolecular forces between the molecules in the liquid medium, forming a cavity. As the cavity grows it becomes unstable and collapses, creating a hotspot where temperatures of around 5000 K and pressures around 1000 atm can be reached [9].

3.2. Microstructure

[fig 3. near here]

To assess the turmeric concentration of the deposits, the carbon content was obtain using GDOES. GDOES depth profiles of the copper electrodeposits are shown in Fig 3. The carbon spike observed at the surface of the deposits is likely due to organic surface contaminates. The electrodeposit produced from the electrolyte with 1.0 g/L of turmeric exhibited the highest carbon content at approximately 3 %. An increase in electrolyte turmeric concentration to 5.0 g/L, produced an electrodeposit with reduced carbon content at approximately 2%. When the electrolyte concentration was increased to 10.0 g/L, whilst turmeric particle size maintained within error of the 5.0 g/L solution by increasing sonication power to 33 W/L, a further significant reduction in deposit carbon content was observed. The results show that the turmeric concentration in the electrolyte was primary factor influencing deposit particle content. The literature shows generally an increase in particle content is observed with increasing electrolyte particle concentration until a saturation point is reached, after which a plateau or small reduction is seen [15-19]. However, a few studies have shown increasing electrolyte particle concentration can reduce the particle content of the electrodeposit [20-22]. The electrocodeposition of inert particles is achieved through several stages. On the addition of the particles to an electrolyte, an ionic cloud is formed around them. The particles are then transported to the cathode by a combination of convection, diffusion, and electrophoresis; whereupon they are weakly absorbed, the ionic cloud is lost and they are strongly absorbed. The particles are then entrapped by the growing metal matrix [23-25]. The literature shows that many factors influence the particle content of an electrodeposit, such as, electrolyte composition, temperature, pH, additives, and agitation, all of which remained consistent [25]. Although no zeta potential analysis was conducted in this research, zeta potential has also been shown to influence deposit particle content [26-28]. It is known increasing particle content in the electrolyte can decrease particle zeta potential (less ionic species are available

to form ionic clouds around the particles), this can reduced particle transport to the cathode, increase particle aggregation, and reduce the particle content of the electrodeposit [29,30].

SEM was used to examine the surface of the electrodeposits. The SEM micrographs of the copper electrodeposits are shown in Fig 4. The pure copper electrodeposit exhibited a relatively smooth and uniform surface texture. Surface nodules were visible on the surface of all electrodeposits with Tween 20 and/or turmeric. Although the deposit produced from the electrolytes containing 5.0 g/L and 10.0 g/L were similar, the nodules observed in the deposit produced from the electrolyte with 10.0 g/L of turmeric were less pronounced. Nodulation is common in electrodeposits and can be attributed to uneven cathodic current distribution. The literature shows an uneven current distribution can be caused by both the presence of surfactants and suspended particles in an electrolyte [31-34].

[fig 4. fig 5. and fig 6. near here]

FIB-SEM was conducted to evaluate the microstructure of the copper electrodeposits. Ion beam micrographs of the copper electrodeposits cross-section are shown in Fig 5. with grain size data calculated from the line intercept method shown in Table 1. The pure copper electrodeposit contained mainly columnar crystals of high aspect ratios. When 10.0 ml/L of Tween 20 was added to the electrolyte, irregular grain morphology with a reduction in grain size was observed. Smaller grains were observed with the addition of 1.0 g/ L of turmeric to the electrolyte. Further grain refinement was observed in the deposit produced from electrolytes containing 5.0 g/L of turmeric. Similar grain refinement was observed when the electrolyte concentration was increased to 10.0 g/L but the particle size maintained within error by increasing sonication power to 33 W/L, despite the observed large reduction in deposit particle content.

Micrographs of the electrodeposit’s cross-section showing the incorporated turmeric particles/cavities are presented in Fig 6. with the mean particle/ cavity size presented in Table

1. The mean particle/cavity size in all electrodeposits exhibited a close correlation to the mean Z-average size of the turmeric particles in the electrolyte. Fewer particles/cavities were visible in the electrodeposit produced from the electrolyte containing 10.0 g/L of turmeric sonicated at 33 W/L, which is consistent with GDOES data.

[table 1. near here]

The results show that particles of a z-average size of 289 ± 30 nm and 278 ± 15 nm, had a greater refinement effect on the grain size of the electrodeposits than particles of 134 ± 37 nm even at much higher deposit particle content. During the electrodeposition of copper, copper ions are transported to the cathode whereupon they obtain two electrons and are reduced onto the substrate. Two important forces occur during this process, Coulomb force, and interfacial tension [35-37]. Generally electrical charge does not homogeneously disperse over the surface of a cathode, creating peaks and troughs. According to Coulomb theory copper ions will be more strongly attracted to the peaks, where they will then be reduced. However, after the ions are reduced, interfacial tension causes the adatoms to defuse away from the peaks (reducing the surface energy of the electrodeposit), this can induce crystal defect such as stacking faults [35]. Grain refinement in electrodeposited copper can be achieved in several ways. The introduction of organic additives (such as Tween 20) to the electrolyte can increase interfacial tension, increasing the diffusion rate of the adatoms from the peaks, and increasing the number of crystal defects. Increasing current density allows less time for the diffusion of the adatoms to occur, therefore at lower current densities a greater number of crystal defects is achieved [35, 36]. Increasing deposit strain can lead to higher dislocation density, and greater grain refinement. Again this can be increased by the introduction of organic additives to the electrolyte or a decrease in cathodic current density [35, 37]. The incorporation of inert particles into an electrodeposit, as also been shown to have a refining effect on grain structure [25,38-41]. The absorption of an inert particle onto the cathode forms a barrier to the

reduction of copper ions at that point, disrupting crystal growth. Turmeric particles of Z-average sizes of 289 ± 30 nm and 278 ± 15 nm, may form a more effective barrier to the reduction of copper ions onto the growing crystal underneath, than turmeric particles of a Z-average size 134 ± 37 nm.

3. Properties

[fig 7. and fig 8. near here]

The Vicker's hardness of the copper electrodeposits is shown in Fig 7. The lowest hardness value was exhibited from the pure copper electrodeposit. An increase in hardness was observed when 10.0 ml/L of Tween 20 was added to the electrolyte. All deposits containing turmeric showed an increase in hardness, with the deposits produced from the electrolyte containing 5.0 g/L and 10.0 g/ l of turmeric sonicated at 33 W/L exhibiting similar hardness. The increase in hardness observed in the deposits containing Tween 20 and turmeric was due to grain structure refinement. Grain size is known to be a major factor affecting the hardness of an electrodeposit [42-53]. Research has shown that a reduction in grain size leads to increased hardness in electrodeposits. As grain size is reduced the number of grain boundaries increase, dislocations are forced to build up at these grain boundaries until sufficient energy is achieve to initiate slip, the larger the grain the more quickly this is achieved [48,52,53].

The copper electrodeposits WCA values are shown in Fig 8. The pure copper electrodeposit displayed wetting behaviour (having a WCA <90°) with the lowest WCA of the electrodeposits. An increase in WCA was observed when 10.0 ml/L of Tween 20 was added to the electrolyte. Again all deposits containing turmeric showed a decrease in wetting behaviour, with the deposits produced from the electrolytes containing 5.0 g/L and 10.0 g/ l of turmeric sonicated at 33 W/L, exhibiting similar WCA. The surface energy of an electrodeposit is known to be a major factor influencing its wetting behaviour. The surface energy can be affected by particle content, grain size, crystallographic orientation and surface

roughness [54-57]. The WCA values of the copper electrodeposits showed good correlation to their grain size, indicating that this was the primary factor influencing their wetting behaviour.

[fig 9. and fig 10. near here]

Photographic salt spray images of the copper electrodeposits are shown in Fig 9. with their weight loss calculated corrosion rates shown in Fig 10. Visual inspection after 240 hours showed corrosion in all copper electrodeposits, with the electrodeposits containing turmeric exhibiting greater corrosion. The dark red areas of the electrodeposits can be attributed to copper (I) oxide (Cu_2O), the black areas can be attributed to copper (II) oxide (CuO), with the green areas attributed to localised corrosion caused by corrosive ions [56]. The white areas were likely due to the corrosion products of zinc (ZnO and $Zn(OH)_2$) from the brass substrate, caused by the failure of the copper coating allowing oxygen and moisture to reach the brass substrate underneath [57]. All copper electrodeposits containing turmeric showed an enhanced corrosion rate when compared to the pure copper electrodeposit and the copper electrodeposited from the electrolyte with only Tween 20. This is in contrast to what has been observed in past research on nickel turmeric composites [8]. The cathodic and anodic corrosion half cells for the copper electrodeposits is shown in equations 6 and 7 respectively. Self-ionisation of pure water is low, leading to relatively slow corrosion. However, the inclusion of NaCl improves conductivity, substantially increasing the rate of corrosion [58,59].

$$O_{2(g)} + 4H^{+}_{(aq)} + 4e^{-} = 2H_2O_{(l)} \quad (6)$$

$$Cu_{(s)} = Cu^{2+}_{(aq)} + 2e^{-} \quad (7)$$

On exposure to air the surface of a metal is coated by an oxide film, however once submerged in an aqueous medium the oxide film can dissolve revealing the bare metal underneath. The solubility of the oxide film is less in near-neutral solutions compared to acidic solutions. If a

near-neutral solvent contains inhibiting ions the solubility of the oxide film may be suppressed, the oxide film may stabilise to form a passive layer (which prevents corrosion), placing the metal in a passive state. In a passive environment grain refinement reduces the metals corrosion rate [59]. However, oxide films are usually less substantial at incursions (such as turmeric particles), thus initially the underlying metal is exposed there first in localised areas. The literature shows that the incorporation of inert particles into a electrodeposit can cause weak points around the embedded particles. These weak points allow the electrolyte to penetrate deep into the electrodeposit accelerating corrosion [31, 60]. Although the copper electrodeposits containing turmeric exhibited grain refinement, the extent of this was not sufficient to overcome the weak points imparted by the embedded turmeric particles, therefore an increase in corrosion rate was observed. The contrast between the corrosion behaviour of copper turmeric coatings and nickel turmeric coatings reported in the literature, can be explained by the grain structure of the nickel deposits [8]. Nickel has naturally greater corrosion resistance than copper, and the extent of grain refinement achieved from the incorporation of turmeric into the nickel deposits was much greater than that achieved for copper, Therefore, an overall decrease in corrosion rate was observed.

4. Conclusions

The microstructure and properties of copper electrodeposited composites incorporating various turmeric particle sizes and concentrations were examined. The turmeric content of the electrodeposits showed a reverse correlation to the concentration of turmeric in the electrolyte. This was likely due to the change in zeta potential of the turmeric particles with increasing turmeric concentration. Microstructural analysis showed that turmeric particle Z-average size had a greater influence on grain refinement than the concentration of turmeric in the electrodeposit. It was found that greater grain refinement was achieved when turmeric particles with a Z-average size of 289 ± 30 nm and 278 ± 15 nm were used, when compared to turmeric particles with a Z-average size of 134 ± 37 nm. Grain size refinement led to a

significant increase in both hardness and WCA. However, the incorporation of turmeric into the electrodeposit also led to weak points in the coating allowing deeper penetration of the electrolyte and a decrease in resistance to salt spray corrosion. For applications where an increase in hardness or hydrophobic behaviour is needed (such as self cleaning surfaces, and more durable heat exchangers and PCB's), the use of turmeric as a filler particle may be a suitable sustainable substitute to some of the more frequently used particles. However, for applications where the corrosion rate of copper in a salt spray environment is a concern (such as marine coatings), the use of turmeric as a filler particle in copper may not be suitable.

5. References

[1] M.F. Ashby, K. Johnson, Materials and Design: The Art and Science of Material Selection in Product Design, Butterworth-Heinemann, 2013.

[2] H. Holleck, Material selection for hard coatings, Journal of Vacuum Science & Technology A: Vacuum, Surfaces, and Films. 4 (1986) 2661-2669.

[3] SEAC Special interest group, Time for strategic change: UK Surface Engineering and Advanced Coatings Industry, A report by the SEAC Special interest group. (2014) 1-44.

[4] M. Antonijevic, M. Petrovic, Copper corrosion inhibitors. A review, International Journal of Electrochemical Science. 3 (2008) 1-28.

[5] R. Dalton, G. Diaz, R. Price, A. Zunkel, The cuprex metal extraction process: recovering copper from sulfide ores, JOM. 43 (1991) 51-56.

[6] H. Chiba, T. Ogushi, H. Nakajima, T. Ikeda, Heat transfer capacity of lotus-type porous copper heat sink, JSME International Journal Series B Fluids and Thermal Engineering. 47 (2004) 516-521.

[7] Y. Yang, R. Boom, B. Irion, D. van Heerden, P. Kuiper, H. de Wit, Recycling of composite materials, Chemical Engineering and Processing: Process Intensification. 51 (2012) 53-68.

[8] R.Merrill, L.Wu, J.E.Graves, J.Beddow, E.Fuentes, A.Cobley, A route to a more sustainable nickel composite electrodeposit, using turmeric and a new low nickel ion concentration electrolyte, Surface and Coatings Technology, 380 (2019) 125024.

[9] United States Department of Agriculture Agricultural Research Service, National Nutrient Database for Standard Reference Legacy Release, 02043, Spices, turmeric, ground. 2019 (2018).

[10] M. Nagarnaik, A. Sarjoshi, A. Bodkhe, B. Khanal, M. Pise, G. Pandya, Characterization of active constituents in Turmeric powder and validation of method for curcumin in samples, Asian Journal of Research in Chemistry. 8 (2015) 643-647.#

[11] C.T. Rueden, J. Schindelin, M.C. Hiner, B.E. DeZonia, A.E. Walter, E.T. Arena, K.W. Eliceiri, ImageJ2: ImageJ for the next generation of scientific image data, BMC Bioinformatics. 18 (2017) 529.

[12] I. Tudela, Y. Zhang, M. Pal, I. Kerr, A.J. Cobley, Ultrasound- assisted electrodeposition of composite coatings with particles, Surface and Coatings Technology. 259 (2014) 363-373.

[13] O. Louisnard, J. González-García, Acoustic cavitation (Eds.), Springer, New York-Dordrecht-Heidelberg-London, 2011. in: H. Feng, G. Barbosa-Canovas, J. Weiss (Eds.), Ultrasound Technologies for Food and Bioprocessing, Springer, New York, Dordrecht, Heidelberg, London, 2011.

[14] J.E. Graves, M. Sugden, R.E. Litchfield, D.A. Hutt, T.J. Masonc , A.J. Cobley, Ultrasound Assisted Dispersal of a Copper Nanopowder for Electroless Copper Activation. Ultrasonics Sonochemistry. 29 (2016) 428-438

[15] D. Iacovetta, J. Tam, U. Erb, Synthesis, structure, and properties of superhydrophobic nickel-PTFE nanocomposite coatings made by electrodeposition, Surf. Coat. Technol. 279 (2015) 134.

[16] V. Medeliene, A. Kosenko, Structural and functional properties of electrodeposited copper metal matrix composite coating with inclusions of WC, Mater.Sci. 14 (2008) 29-33.

[17] V. Medeliene, M. Kurtinaitienė, G. Bikulčius, V. Stankevič, A study of copper coatings electrodeposited in electrolyte with a metallic powder of chromium, Surface and Coatings Technology. 200 (2006) 6123-6129.

[18] K. Rajkumar, S. Aravindan, Tribological studies on microwave sintered copper–carbon nanotube composites, Wear. 270 (2011) 613-621.

[19] Y. Yang, Y. Wang, Y. Ren, C. He, J. Deng, J. Nan, J. Chen, L. Zuo, Single-walled carbon nanotube-reinforced copper composite coatings prepared by electrodeposition under ultrasonic field, Mater Lett. 62 (2008) 47-50.

[20] A. Robin, J. Pinheiro de Santana, A. Fernando Sartori, Co-electrodeposition and characterization of Cu–Si3N4 composite coatings, Surface and Coatings Technology. 205 (2011) 4596-4601.

[21] M. Eslamia, H. Saghafiana, F. Golestani-farda, A. Robin, Effect of electrodeposition conditions on the properties of Cu–Si3N4 composite coatings, Applied Surface Science. 300 (2014) 129–140.

[22] J. Zhu, G.H. Lei Liu, B. Shen, W. Hu, W. Ding, Study on composite electroformingof Cu/SiCp composites, Mater. Lett. 58 (2004) 1634–1637.

[23] J.P. Celis, J.R. Roos, C.:. Buelens, A Mathematical Model for the Electrolytic Codeposition of Particles with a Metallic Matrix, The Electrochemical Society. 134 (1987) 1402-1408.

[24] F.C. Walsh, C.T.J. Low, A review of developments in the electrodeposition of tin, Surf. Coat. Technol. 288 (2016) 79-94.

[25] F. C. Walsh* C. Ponce de Leon., A review of the electrodeposition of metal matrix composite coatings by inclusion of particles in a metal layer: an established and diversifying technology, Transactions of the IMF. 92 (2014) 83-98.

[26] P. Narasimman, M. Pushpavanam, V. Periasamy, Wear and scratch resistance characteristics of electrodeposited nickel-nano and micro SiC composites, Wear. 292 (2012) 197-206.

[27] A. Sohrabi, A. Dolati, M. Ghorbani, A. Monfared, P. Stroeve, Nanomechanical properties of functionally graded composite coatings: Electrodeposited nickel dispersions containing silicon micro-and nanoparticles, Mater. Chem. Phys. 121 (2010) 497-505.

[28] P. Gyftou, M. Stroumbouli, E. Pavlatou, P. Asimidis, N. Spyrellis, Tribological study of Ni matrix composite coatings containing nano and micro SiC particles, Electrochim. Acta. 50 (2005) 4544-4550.

[29] E. Saka, C. Güler, The effects of electrolyte concentration, ion species and pH on the zeta potential and electrokinetic charge density of montmorillonite, Clay Miner. 41 (2006) 853-861.

[30] R. Sprycha, Electrical double layer at alumina/electrolyte interface: I. Surface charge and zeta potential, J. Colloid Interface Sci. 127 (1989) 1-11.

[31] M. Lekka, D. Koumoulis, N. Kouloumbi, P. Bonora, Mechanical and anticorrosive properties of copper matrix micro-and nano-composite coatings, Electrochimica Acta. 54 (2009) 2540-2546.

[32] N.Shrestha, T, Takebe. T, Saji. Effect of particle size on the co-deposition of diamond with nickel in presence of a redox-active surfactant and mechanical property of the coatings, Diamond and Related Materials. 15 (2006) 1570-1575

[33] I. Garciaab, J. Fransaera, J. Celisa Electrodeposition and sliding wear resistance of nickel composite coatings containing micron and submicron SiC particles, Surface and Coatings Technology. 148 (2001) 171-178.

[34] A. Sohrabi, A. Dolati, M. Ghorbani, A. Monfared, P. Stroeve. Nanomechanical properties of functionally graded composite coatings: Electrodeposited nickel dispersions containing silicon micro- and nanoparticles, Materials Chemistry and Physics. 121 (2010) 497-505.

[35] G. Wang, Z. Jiang, J. Lian, Q. Jiang, The grain refinement mechanism of electrodeposited copper, Journal of Materials Research. 24 (2009) 3226-3236.

[36] W. Zhao, N. Tao, J. Guo, Q. Lu, K. Lu, High density nano-scale twins in Cu induced by dynamic plastic deformation, Scripta Materialia. 53 (2005) 745.

[37] G. Gray III, P. Follansbee, C. Frantz, Effect of residual strain on the substructure development and mechanical response of shock-loaded copper, Materials Science and Engineering. 9 (1989) 111.

[38] N. Qu, D. Zhu, K. Chan, Fabrication of Ni–CeO2 nanocomposite by electrodeposition, Scripta Materialia. 54 (2006) 1421-1425.

[39] H. Algul, M. Tokur, S. Ozcan, M. Uysal, T. Cetinkaya, H. Akbulut, A. Alp, The effect of graphene content and sliding speed on the wear mechanism of nickel–graphene nanocomposites, Applied Surface Science. 359 (2015) 340-348.

[40] J. Li, Y. Sun, X. Sun, J. Qiao, Mechanical and corrosion-resistance performance of electrodeposited titania–nickel nanocomposite coatings, Surface and Coatings Technology. 192 (2005) 331-335.

[41] S. Spanou, E. Pavlatou, N. Spyrellis, Ni/nano-TiO2 composite electrodeposits: Textural and structural modifications, Electrochimica Acta. 54 (2009) 2547-2555.

[42] Q. Zhang, Y. Liu, Y. Liu, Y. Ren, Y. Wu, Z. Gao, X. Wu, P. Han, Enhanced tensile ductility and strength of electrodeposited ultrafine-grained nickel with a desired bimodal microstructure, Materials Science & Engineering A; Materials Science & Engineering A. 701 (2017) 196-202.

[43] J. Lohmiller, M. Grewer, C. Braun, A. Kobler, C. Kübel, K. Schüler, V. Honkimäki, H. Hahn, O. Kraft, R. Birringer, P.A. Gruber, Untangling dislocation and grain boundary mediated plasticity in nanocrystalline nickel, Acta Materialia. 65 (2014) 295-307.

[44] K. Schüler, B. Philippi, M. Weinmann, V.M. Marx, H. Vehoff, Effects of processing on texture, internal stresses and mechanical properties during the pulsed electrodeposition of nanocrystalline and ultrafine-grained nickel, Acta Materialia. 61 (2013) 3945-3955.

[45] A. Rashidi, A. Amadeh, The effect of saccharin addition and bath temperature on the grain size of nanocrystalline nickel coatings, Surface and Coatings Technology. 204 (2009) 353-358.

[46] R. Mishra, B. Basu, R. Balasubramaniam, Effect of grain size on the tribological behavior of nanocrystalline nickel, Materials Science and Engineering: A. 373 (2004) 370-373.

[47] J. Schiøtz, F.D. Di Tolla, K.W. Jacobsen, Softening of nanocrystalline metals at very small grain sizes, Nature. 391 (1998) 561.

[48] N. Krasilnikov, W. Lojkowski, Z. Pakiela, R. Valiev, Tensile strength and ductility of ultra-fine-grained nickel processed by severe plastic deformation, Materials Science and Engineering: A. 397 (2005) 330-337.

[49] G. Hughes, S. Smith, C. Pande, H. Johnson, R. Armstrong, Hall-Petch strengthening for the microhardness of twelve nanometer grain diameter electrodeposited nickel, Scripta Metallurgica. 20 (1986) 93-97.

[50] Z. Ren, N. Meng, K. Shehzad, Y. Xu, S. Qu, B. Yu, J. Luo, Mechanical properties of nickel-graphene composites synthesized by electrochemical deposition, Nanotechnology. 26 (2015) 065706.

[51] N. Hansen, Hall–Petch relation and boundary strengthening, Scr. Mater. 51 (2004) 801-806.

[52] E.O. Hall, Proc Phys Soc London B. 64 (1951).

[53] N.J. Petch, J Iron Steel Inst. 174 (1953).

[54] L. Vitos, A. Ruban, H.L. Skriver, J. Kollar, The surface energy of metals, Surf. Sci. 411 (1998) 186-202.

[55] M. McLean, Determination of the surface energy of copper as a function of crystallographic orientation and temperature, Acta Metallurgica. 19 (1971) 387-393.

[56] R.N. Wenzel, Surface roughness and contact angle. J. Phys. Chem. 53 (1949) 1466-1467.

[57] A. Cassie, S. Baxter, Wettability of porous surfaces, Transactions of the Faraday society. 40 (1944) 546-551.

[58] L. Bonin, V. Vitry, F. Delaunois, Corrosion behaviour of electroless high boron-mid phosphorous nickel duplex coatings in the as-plated and heat-treated states in NaCl, H2SO4, NaOH and Na2SO4 media, Mater. Chem. Phys. 208 (2018) 77-84.

[59] J. Popplewell, R. Hart, J. Ford, The effect of iron on the corrosion characteristics of 90-10 cupro nickel in quiescent 3· 4% NaCl solution, Corros. Sci. 13 (1973) 295-309.

[60] K. Ralston, N. Birbilis, Effect of grain size on corrosion: a review, Corrosion. 66 (2010) 075005-075005-13.

Table 1. Grain sizes of copper turmeric samples obtained by the line intercept method from the ion beam images. (A) pure Cu. (B) Cu 10.0 ml/L of Tween 20. (C) Cu 10.0 ml/L of Tween 20 and 1.0 g/l of turmeric sonicated at 11 W/L. (D) Cu 10.0 ml/L of Tween 20 and 5.0 g/l of turmeric sonicated at 11 W/L. (E) Cu 10.0 ml/L of Tween 20 and 10.0 g/L of turmeric sonicated at 33 W/L.

Sample	Grain size in Y-axis direction /nm	Grain size in X-axis direction /nm	Mean deposit particle / particle cavity size / nm	Z-average size turmeric /nm
A	662 ± 77	437 ± 26	NA	NA
B	523 ± 55	395 ± 44	NA	NA
C	328 ± 27	234 ± 4	130 ± 14	134 ± 37
D	259 ± 23	233 ± 13	316 ± 128	289 ± 30
E	321 ± 18	283 ± 6	293 ± 35	278 ± 15

Fig 1. The experimental set up during electrodeposition of copper deposits.

Fig 2. The Z-average size of turmeric particles in solution at varying concentrations dispersed by ultrasound for 20 min. (A) Cu electrolyte mimic 1.0 g/l of turmeric sonicated at 11 W/L.(B) Cu electrolyte mimic 5.0 g/l of turmeric sonicated at 11 W/L. (C) Cu electrolyte mimic 10.0 g/l of turmeric sonicated at 11 W/L. (D) Cu electrolyte mimic 10.0 g/l of turmeric sonicated at 33 W/L.

Fig 3. GDOES depth profile of the copper deposits. (A) Cu 10.0 ml/L of Tween 20. (B) Cu 10.0 ml/L of Tween 20 and 1.0 g/l of turmeric sonicated at 11 W/L. (C) Cu 10.0 ml/L of Tween 20 and 5.0 g/l of turmeric sonicated at 11 W/L. (D) Cu 10.0 ml/L of Tween 20 and 10.0 g/L of turmeric sonicated at 33 W/L.

Fig 4. SEM images of the surface of the copper deposits. (A) pure Cu. (B) Cu 10.0 ml/L of Tween 20. (C) Cu 10.0 ml/L of Tween 20 and 1.0 g/l of turmeric sonicated at 11 W/L. (D) Cu 10.0 ml/L of Tween 20 and 5.0 g/l of turmeric sonicated at 11 W/L. (E) Cu 10.0 ml/L of Tween 20 and 10.0 g/l of turmeric sonicated at 11 W/L. (F) Cu 10.0 ml/L of Tween 20 and 10.0 g/L of turmeric sonicated at 33 W/L.

Fig 5. Ion beam images of the cross-section of the copper deposits. (A) pure Cu. (B) Cu 10.0 ml/L of Tween 20. (C) Cu 10.0 ml/L of Tween 20 and 1.0 g/l of turmeric sonicated at 11 W/L. (D) Cu 10.0 ml/L of Tween 20 and 5.0 g/l of turmeric sonicated at 11 W/L. (E) Cu 10.0 ml/L of Tween 20 and 10.0 g/L of turmeric sonicated at 33 W/L.

Fig 6. Electron beam images of cavities / particles in the cross-section of the copper deposits obtained by FIB-SEM. (A) Cu 10.0 ml/L of Tween 20 and 1.0 g/l of turmeric sonicated at 11 W/L. (B) Cu 10.0 ml/L of Tween 20 and 5.0 g/l of turmeric sonicated at 11 W/L. (C) Cu 10.0 ml/L of Tween 20 and 10.0 g/L of turmeric sonicated at 33 W/L.

Fig 7. Mean hardness of Cu deposits tested with a Vicker's indenter. (A) pure Cu. (B) Cu 10.0 ml/L of Tween 20. (C) Cu 10.0 ml/L of Tween 20 and 1.0 g/l of turmeric sonicated at 11 W/L. (D) Cu 10.0 ml/L of Tween 20 and 5.0 g/l of turmeric sonicated at 11 W/L. (E) Cu 10.0 ml/L of Tween 20 and 10.0 g/L of turmeric sonicated at 33 W/L.

Fig 8. Mean WCA of the copper deposits produced from the various electrolytes. (A) pure Cu. (B) Cu 10.0 ml/L of Tween 20. (C) Cu 10.0 ml/L of Tween 20 and 1.0 g/l of turmeric sonicated at 11 W/L. (D) Cu 10.0 ml/L of Tween 20 and 5.0 g/l of turmeric sonicated at 11 W/L. (E) Cu 10.0 ml/L of Tween 20 and 10.0 g/L of turmeric sonicated at 33 W/L.

Fig 9. Photographic image of Cu deposit after salt spray analysis, produced from the various electrolytes. (A) pure Cu. (B) Cu 10.0 ml/L of Tween 20. (C) Cu 10.0 ml/L of Tween 20 and 1.0 g/l of turmeric sonicated at 11 W/L. (D) Cu 10.0 ml/L of Tween 20 and 5.0 g/l of

turmeric sonicated at 11 W/L. (E) Cu 10.0 ml/L of Tween 20 and 10.0 g/L of turmeric sonicated at 33 W/L.

Fig 10. Corrosion rate of the Cu deposits calculated by mass loss. (A) pure Cu. (B) Cu 10.0 ml/L of Tween 20. (C) Cu 10.0 ml/L of Tween 20 and 1.0 g/l of turmeric sonicated at 11 W/L. (D) Cu 10.0 ml/L of Tween 20 and 5.0 g/l of turmeric sonicated at 11 W/L. (E) Cu 10.0 ml/L of Tween 20 and 10.0 g/L of turmeric sonicated at 33 W/L.

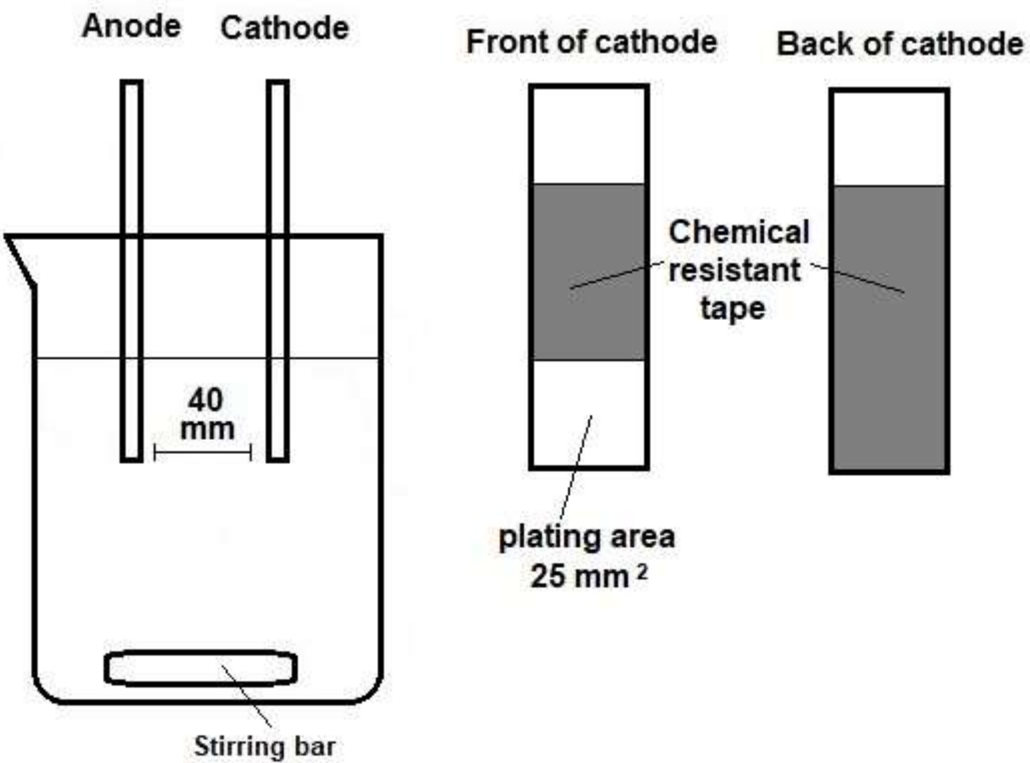

Fig 1.

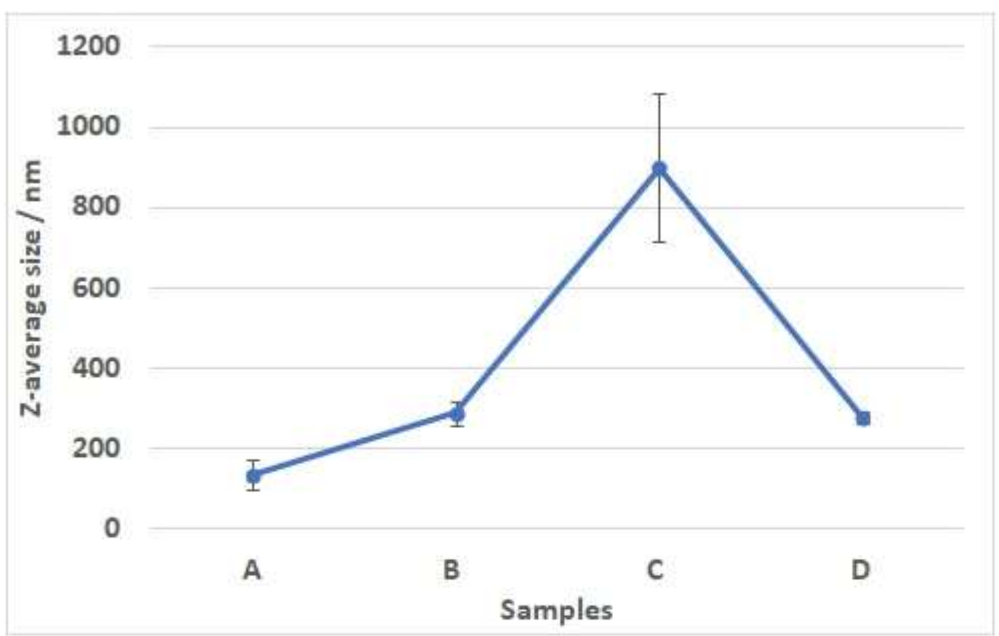

Fig 2.

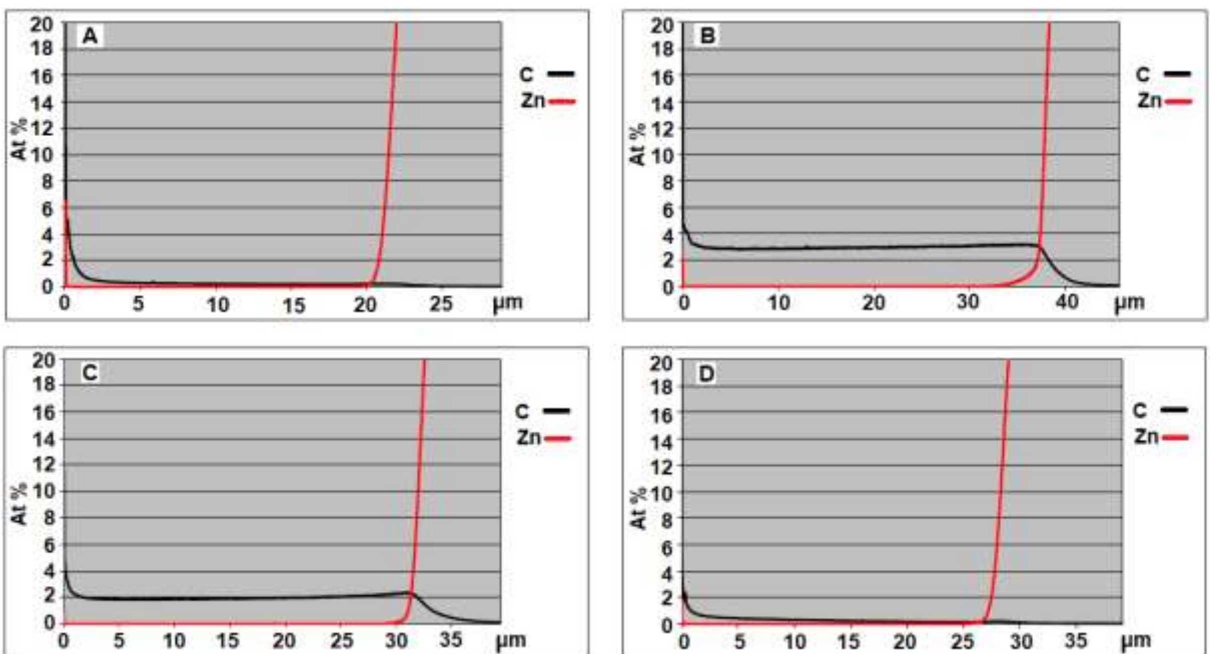

Fig 3.

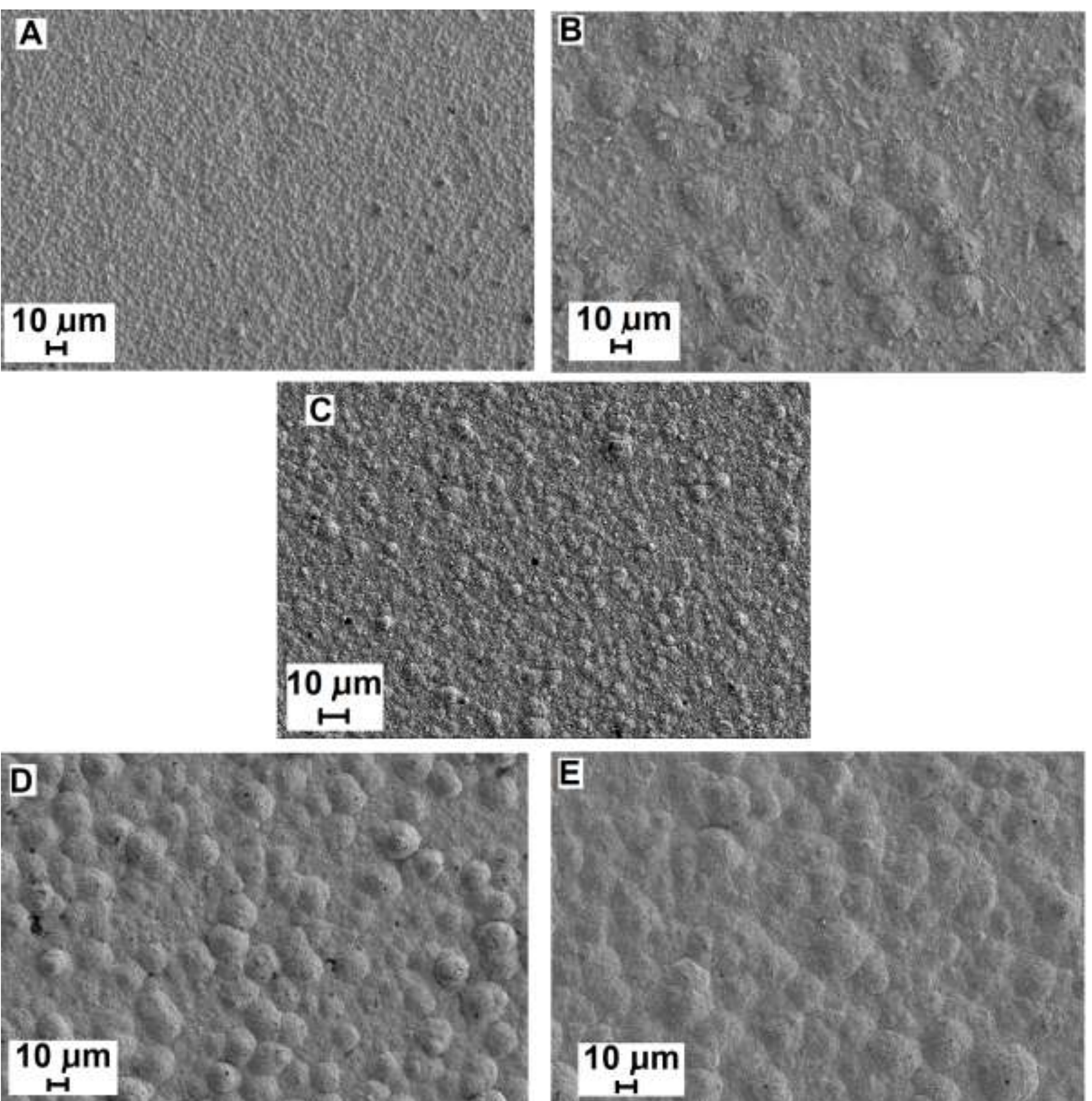

Fig 4.

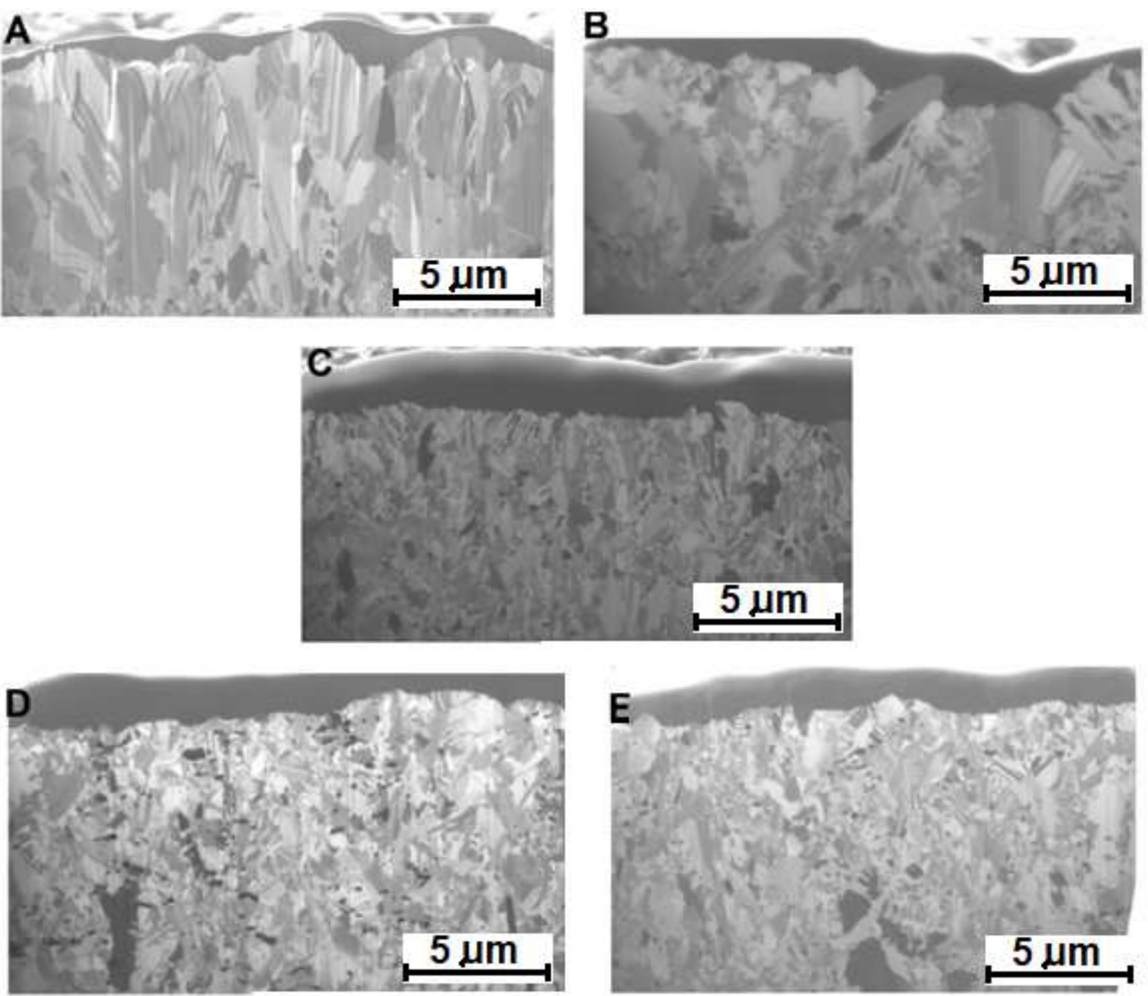

Fig 5.

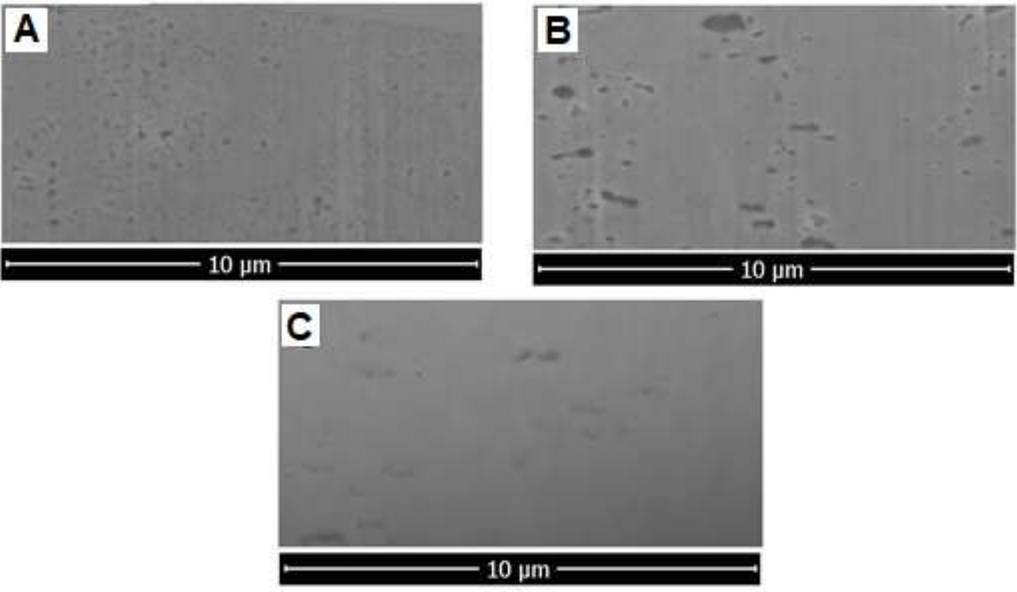

Fig 6.

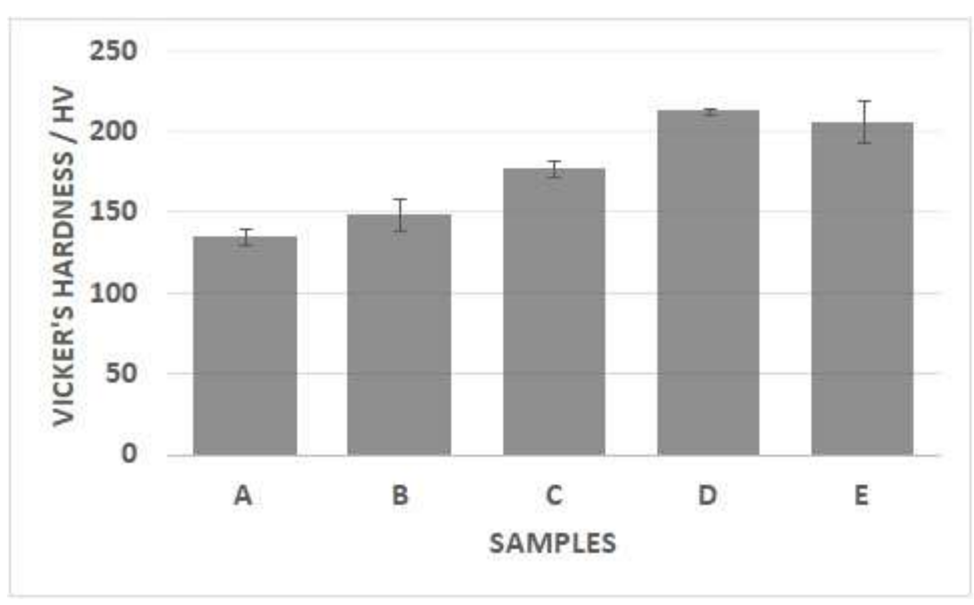

Fig 7.

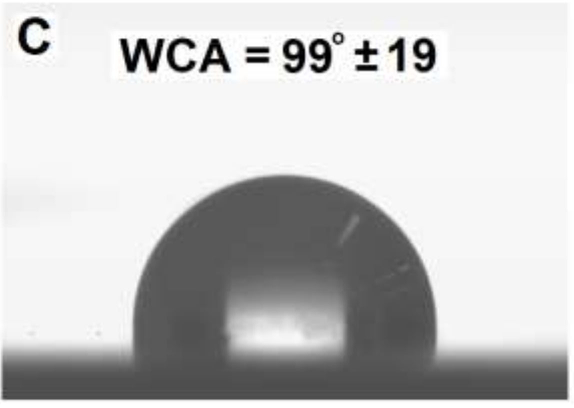

Fig 8.

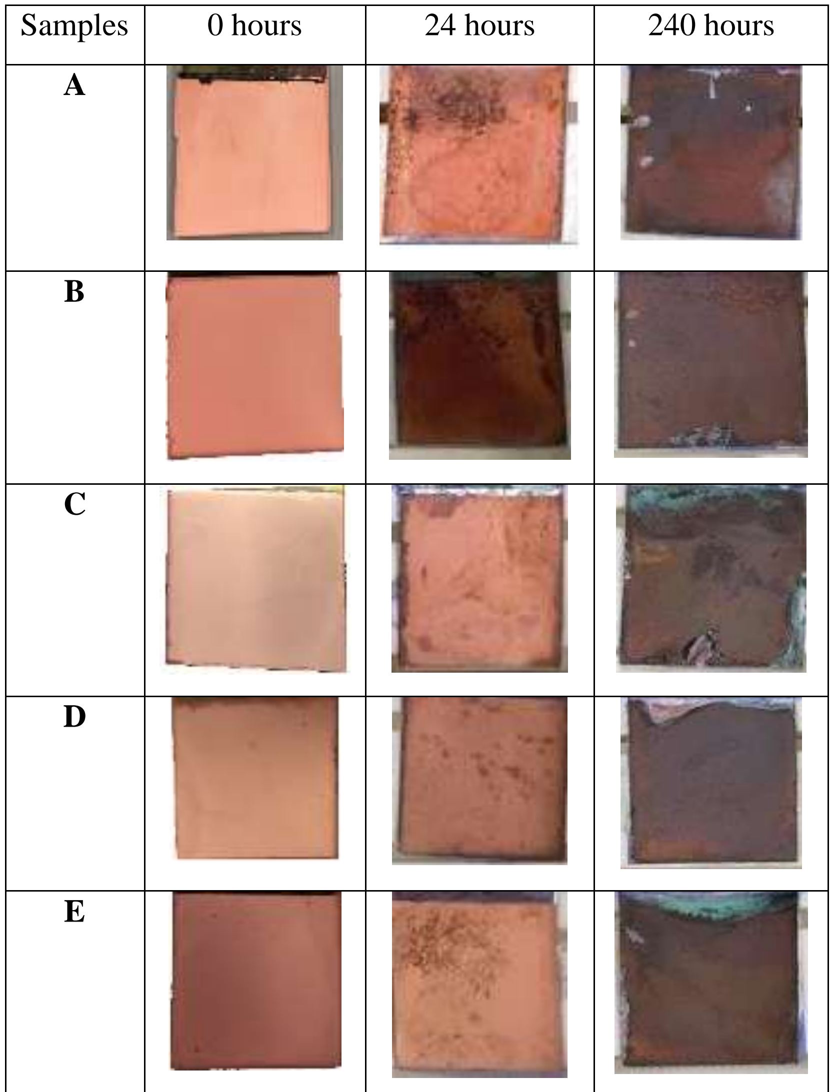

Fig 9.

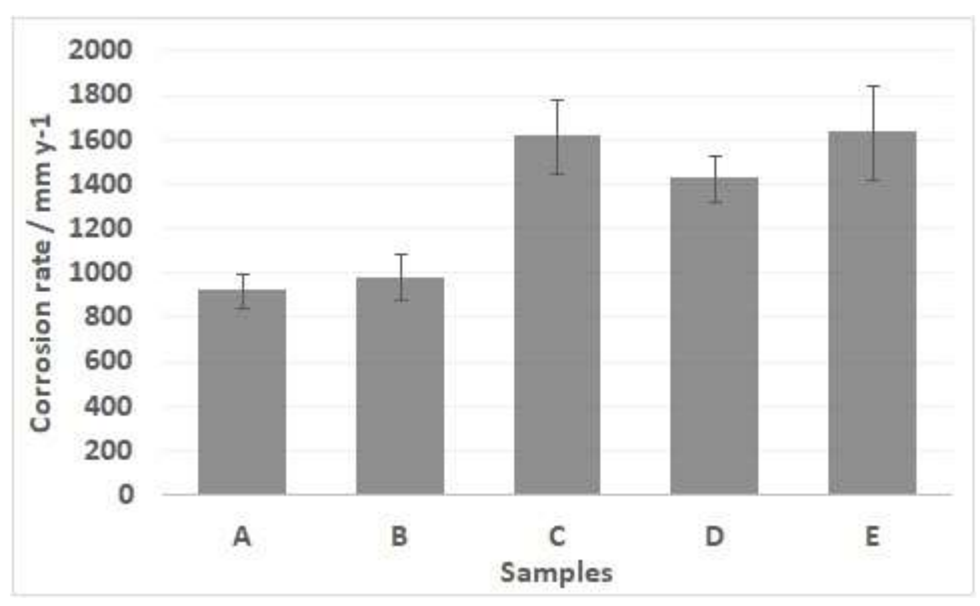

Fig 10.

Word count 3526